Epitaxy of single crystalline PrO_2 films on Si(111)

T. Weisemoeller,[1] C. Deiter,[1] F. Bertram,[1] S. Gevers,[1] A. Giussani,[2] P. Zaumseil,[2] T. Schroeder,[2] and J. Wollschläger[1,a)]

[1]*Department of Physics, University of Osnabrück, Barbarastrasse 7, D-49069 Osnabrück, Germany*
[2]*IHP, Im Technologiepark 25, 15236 Frankfurt (Oder), Germany*

(Received 23 February 2008; accepted 23 June 2008; published online 24 July 2008)

A film of praseodymium sesquioxide with hexagonal structure, that has been deposited on Si(111) by molecular beam epitaxy, was annealed in oxygen atmosphere to obtain a PrO_2 film for improved heteroepitaxy as buffer dielectric for alternative semiconductor layer integration. The film structure is characterized by x-ray diffraction and x-ray reflectometry. The film is single crystalline with $Fm\bar{3}m$ (fluorite) structure. It is B oriented with respect to Si and has lattice constants close to bulk PrO_2. The cubic lattice of the PrO_2 film is slightly distorted due to residual oxygen vacancies which increase the diameter of Pr ions. © *2008 American Institute of Physics*. [DOI: 10.1063/1.2958227]

Rare earth oxides are of continued interest for both industrial and scientific research. For instance, these materials have been discussed in the context of electro-optics,[1] sensor technology,[2] and microelectronics.[3] In the latter field, especially heteroepitaxial rare earth oxide thin films on silicon attract increasing research interest. For example, single crystalline oxides on silicon systems are discussed as highly functional buffer oxide structures to achieve the global integration of alternative semiconductors on Si [engineered silicon wafers, e.g., Ge/PrO_2,[4] InP/Gd_2O_3[5]]. Another key technology is the local integration of epitaxial rare earth oxides on Si to improve the performance of future Si device technologies (e.g., high-k oxides for complementary metal oxide semiconductor applications).[6]

Here one candidate is praseodymium oxide. Hexagonal h-Pr_2O_3 forms crystalline thin films on clean Si(111) surfaces with good *lateral* lattice matching (+0.5% lattice mismatch), but is unstable if exposed to air.[7] Postdeposition annealing in 10^{-5} mbar O_2 transforms h-Pr_2O_3 films into cubic c-Pr_2O_3 films with bixbyite structure ($Ia\bar{3}$) which are stable if exposed to air.[8] The bulk lattice constant of c-Pr_2O_3 is approximately twice the bulk lattice constant of Si. The residual lattice mismatch is +2.6% taking into account the 2:1 relationship of the lattice constants. The bixbyite structure of c-Pr_2O_3 can be considered as fluorite structure with periodically arranged oxygen vacancies.[9] The anion sublattice of c-$Pr_2O_3(111)$ films forms antiphase boundaries (APBs) on Si(111) since the size of the surface unit cell of c-$Pr_2O_3(111)$ is four times the size of Si(111) surface unit cell. APBs are disadvantageous in the field of heteroepitaxy, as reported for other oxide films.[10] These disadvantages are avoided by PrO_2 films since PrO_2 has fluorite structure and is lattice matched to Si (lattice mismatch −0.7%).

An ultrathin h-Pr_2O_3 film was deposited on Si(111) following the recipe previously reported.[11] Afterward, the sample was removed from the chamber and annealed for 30 min at 450° in 1 atm O_2 to obtain PrO_2. At HASYLAB (DESY, Germany) both x-ray diffraction (XRD) measurements and x-ray reflectivity (XRR) experiments were performed at beam line W1 while grazing incidence XRD (GIXRD) experiments were carried out at beam line BW2. In the following, H, K, and L values of the indexed *peaks* are chosen with respect to the bulk lattices of the corresponding material and will be referred to as $(HKL)_B$. Labeling of the *axes*, however, does always correspond to the hexagonal Si(111) lattice in surface coordinates $(HKL)_S$.

Figure 1 shows the specular θ-2θ XRD scan [$(00L)_S$ rod]. A sharp and strong Bragg peak of the Si(111) substrate is at $L=1$ [$\mathrm{Si}(001)_S$ corresponding to $\mathrm{Si}(111)_B$]. In addition to the $\mathrm{Si}(111)_B$ peak there is a much broader peak that is caused by the $PrO_2(111)$ film. Close to $L=1$ the diffracted x-ray intensity shows fringes due to interference between Si substrate and deposited film. Intensity oscillations are also observed by XRR (not presented here). Carefull analysis of the XRR data shows that the film has two contributions. The PrO_2 film has 5.3 nm thickness while a silicate film of 1.8 nm thickness is formed at the interface. The silicate formation at the interface is observed by transmission electron microscopy too. Silicate formation has previously been reported for c-Pr_2O_3 films on Si(111) obtained from annealing of h-Pr_2O_3 by annealing in low pressure O_2 atmosphere.[8]

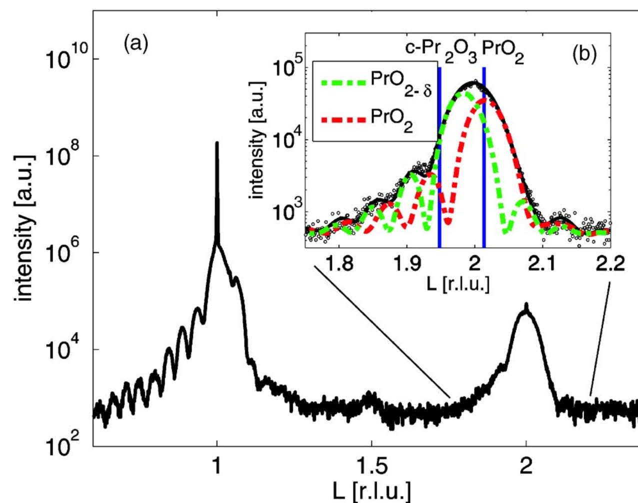

FIG. 1. (Color online) (a) $(00L)_S$ scan. The intensity close to $L=1$ is due to the strong $\mathrm{Si}(111)_B$ peak as well as fringes due to the PrO_2 film. The intensity close to $L=2$ is governed by the PrO_2 film. (b) CTR analysis of the PrO_2 film close to $L=2$. The positions of Bragg peaks due to bulk $PrO_2(222)_B$ as well as c-$PrO_2(444)_B$ are also marked.

[a)]Electronic mail: joachim.wollschlaeger@uos.de.

Author complimentary copy. Redistribution subject to AIP license or copyright, see http://apl.aip.org/apl/copyright.jsp

A very weak XRD peak is observed at $L=1.5$ which cannot be due to c-Pr_2O_3 or due to PrO_2. Bulk h-Pr_2O_3 does fulfill the $(0003)_B$ Bragg condition at $L=1.56$, but can be excluded for this sample as we will see later. The XRD intensity at $L\approx 2$ is dominated by the oxide film since the $Si(222)_B$ is kinematically forbidden. A sharp but weak $Si(222)_B$ peak [corresponding to $Si(002)_S$] can be observed for $L=2$ due to the nonspherical electron density distribution for Si. The Si peak is strong enough to be used for calibration but not so strong that it causes noticeable interference with the praseodymia peak. The analysis of the structure of the PrO_2 film has been carried out with this Bragg peak since there are no complications due to the interference with the Si substrate and the (amorphous) silicate film as for the $Si(111)_B$ Bragg peak.

The data close to $L=2$ are analyzed within the kinematic diffraction theory. Both the vertical lattice constant d and the thickness of the film are the most important parameter to fit the XRD data. Assuming one single layer distance d for the oxide film we obtain only poor agreement between experimental data and the optimized intensity calculations. Therefore the film separates in two parts with different vertical lattice constants d_0 and d_δ. We considered two different models: (1) the nonstoichiometric part of the oxide film (lattice constant d_δ) is closer to the Si substrate than the stoichiometric part with lattice constant d_0 (vertical phase separation) and (2) both parts coexist with lateral phase separation and have the same film thickness. Only the second model of lateral phase separation explains the XRD data in agreement with the XRR data (especially the thickness of 5.3 nm for the oxide film), as demonstrated by Fig. 1(b). Finally, layer distances $d_0=0.3101$ nm and $d_\delta=0.3154$ nm are obtained from the optimized XRD analysis. On the one hand, d_0 almost matches the layer distance of bulk PrO_2 [−0.4% mismatch, cf. PrO_2 peak in Fig. 1(b)] and we attribute this phase to stoichiometric PrO_2. On the other hand, the left XRD peak associated with d_δ is clearly shifted. The vertical lattice mismatch of this species is +1.3% with respect to bulk PrO_2 so that this phase is attributed to nonstoichiometric $PrO_{2-\delta}$ with oxygen vacancies for the anion sublattice. Therefore the oxide film is inhomogeneous and shows two (111) oriented phases with different vertical lattice constants which are laterally separated.

Figure 2 presents a scan in the $(0K0)_S$-direction (in-plane scan), parallel to the surface. The weak peaks at $K=1$ and $K=2$ are due to Si crystal truncation rods (CTRs) while the peak at $K=3$ is the $Si(\bar{2}4\bar{2})_B$ peak. For a sample with c-Pr_2O_3 film, XRD peaks are expected at both $K\approx 1.46$ and $K\approx 2.19$ due to both $(2\bar{4}2)_B$ and $(3\bar{6}3)_B$ Bragg peaks, respectively. As this is not the case for this sample, no c-Pr_2O_3 is formed under the given conditions. However, there is a broad peak at $K=2.985$. This is close to the position of bulk PrO_2 ($K=3.020$). Therefore the lateral unit cell size for the film in $[010]_S$-direction ($[1\bar{2}1]_B$-direction) is 1.17% larger than expected for bulk PrO_2. The same behavior is also observed in the $[100]_S$-direction ($[11\bar{2}]_B$-direction, not shown here). In contrast to the L scan in Fig. 1(b), fitting with two praseodymia peaks in K-or H-direction does not improve results. Thus the praseodymia film shows only one lateral lattice constant although it has two different vertical lattice constants (layer distances). Finally, we conlcude from the full width at half maximum of the oxide peak that the average grain size of the single crystalline PrO_2 film is approximately 11 nm.

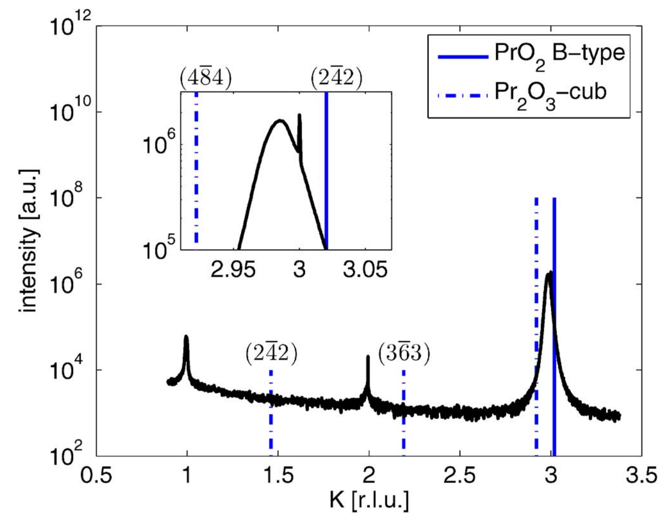

FIG. 2. (Color online) In-plane $(0K0)_S$ scan. Bragg peaks of the PrO_2 film and the Si substrate are at $K=2.985$ and $K=3$, respectively. Si CTRs are at at $K=1$ and $K=2$. Positions of bulk c-Pr_2O_3 and Pr_2O_3 are marked.

Figure 3 shows a $(01L)$ CTR scan. Broad peaks are visible at $L=0.34$ and $L=1.33$. A sharp peak is visible at $L=1.67$ due to the Si substrate. Therefore we can exclude h-Pr_2O_3 which would fulfill Bragg conditions at $L\approx 0.52$, $L\approx 1.04$, and $L\approx 1.56$.[7] Peaks at these positions are obviously *not* observed. A-type and B-type growth stackings (latter rotated by 180° with respect to the substrate) can well be distinguished from this experiment due to different Bragg peak positions. A-type PrO_2 would fulfill Bragg conditions at $L=0.68$ and $L=1.70$ (dashed lines in Fig. 3), while B-type PrO_2 has Bragg peaks at $L=0.34$ and $L=1.36$ (solid lines in Fig. 3). Analyzing the measured intensities for both $L=0.34$ and $L=0.68$ and considering the effects due to different form factors of PrO_2 for both diffraction conditions we conclude that at least more than 99.9% of the PrO_2 film is B oriented. Therefore, the film is single crystalline and B oriented with $Si(\bar{1}2\bar{1})_B \| PrO_2(1\bar{2}1)_B$.

In summary, a B-oriented heteroepitaxial praseodymia film with $Fm\bar{3}m$ structure and with lattice constants close to bulk $PrO_2(111)$ was verified after postdeposition annealing of h-$Pr_2O_3/Si(111)$. Thus we can conclude that the preparation recipe is suitable for single crystalline PrO_2 films on Si(111) with $PrO_2(111)_B \| Si(111)_B$ in vertical direction and

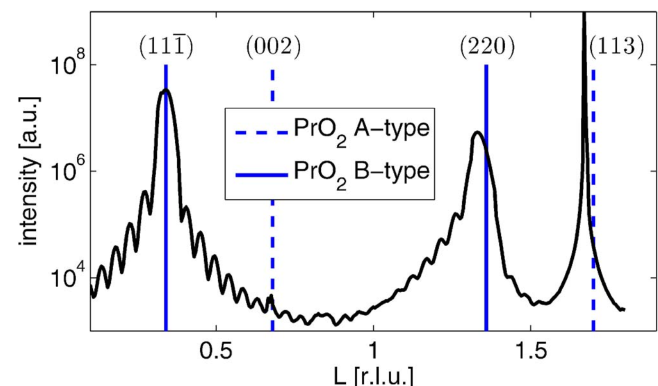

FIG. 3. (Color online) $(01L)_S$ scan. All peaks and fringes are due to B-oriented PrO_2 except the strong peak at $L=5/3$ due to Si.

Author complimentary copy. Redistribution subject to AIP license or copyright, see http://apl.aip.org/apl/copyright.jsp

$PrO_2(1\bar{2}1)_B \| Si(\bar{1}2\bar{1})_B$ in horizontal direction. The prepared film is free of residual c-Pr_2O_3 and h-Pr_2O_3 and does not show any formation of twins.

On the one hand the XRD studies show two different lattice constants in vertical direction pointing to the separation in two phases of the oxide film. One phase (lattice constant d_0) almost matches bulk PrO_2 (with small lattice contraction) while the structure of the other phase (lattice constant d_δ) is vertically expanded. On the other hand a slightly expanded lattice is observed in lateral direction. We assume that the lateral lattice expansion is caused by the silicate film at the interface.

Assuming Poisson's ratio 1/3 for PrO_2 (Ref. 12) the small distortion of PrO_2 (lateral +0.5%, vertical −0.4%) can be explained as elastic deformation of the oxide film as previously reported for $CaF_2/Si(111)$.[13] Taking into account the thermal expansion of both PrO_2 film and Si(111) substrate we can exclude that the distortion of the film is caused by lattice matched phase transformation during annealing in O_2 atmosphere.

It is well known for bulk praseodymia that the decreasing oxidation state of Pr ions due to oxygen vacancies increases both the diameter of Pr ions and the bulk lattice constant of praseodymia.[9] Therefore we associate the phase with d_δ with understoichiometric $PrO_{2-\delta}$. At high temperatures praseodymium can only completely be oxidized at high O_2 pressure so that *bulk* PrO_2 usually has oxygen vacancies.[14,15] Assuming the same effect for epitaxial PrO_2 *films* explains the small oxygen deficit for the oxide film. In addition, we conclude from the oxide Bragg peak at $L=1.5$ that the oxygen vacancies periodically order in vertical direction. The vacancy density of 7% can be quantified comparing the intensity of the oxide Bragg peaks at $L=1.5$ and $L=2$. X-ray photoemission spectroscopy investigations show that the oxide film shows mainly Pr^{4+} ions. It is very difficult to determine the amount of Pr^{3+} ions from Pr3d photoelectron spectra due to final state effects as previously reported.[16] Figure 4 presents a model for $PrO_2/Si(111)$.

The lateral separation into stoichiometric PrO_2 and understoichiometric $PrO_{2-\delta}$ points to the nucleation of PrO_2 during the oxidation process. PrO_2 nucleii, however, do not grow continuously until the entire film has PrO_2 stoichiometry. Instead the interplay of oxidation and reduction determines the amount of stoichiometric and nonstoichiometric oxide.

Thus, having successfully prepared PrO_2 films on Si(111), it is now possible to study in a comparative way the defect characteristics of bixbyite Pr_2O_3 and fluorite PrO_2 heterostructures in Si(111), i.e., in terms of the influence of point defects (oxygen vacancies) as well as extended defects

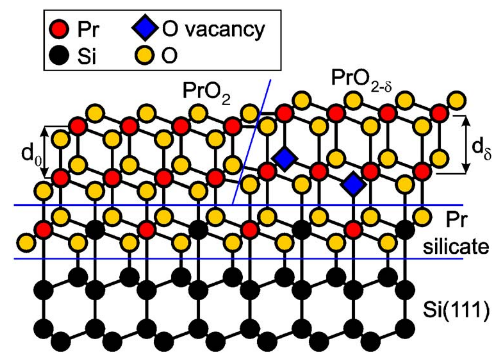

FIG. 4. (Color online) Model for $PrO_2/Si(111)$ with silicate film at the interface and lateral phase separation of PrO_2 (left) and $PrO_{2-\delta}$ (right).

(APBs) on the dielectric properties. These future studies are of utmost importance to evaluate the potential of rare earth oxide heterostructures on Si for the future integration of single crystalline, alternative semiconductor layers with low defect densities.

[1] D. T. Bowron, G. A. Saunders, R. J. Newport, B. D. Rainford, and H. B. Senin, Phys. Rev. B **53**, 5268 (1996).
[2] J. R. Stetter, W. R. Penrose, and S. Yao, J. Electrochem. Soc. **150**, 11 (2003).
[3] J. Kwoet, M. Hong, B. Busch, D. A. Muller, Y. J. Chabal, A. R. Kortan, J. P. Mannaerts, B. Yang, P. Ye, H. Gossmann, A. M. Sergent, K. K. Ng, J. Bude, W. H. Schulte, E. Garfunkel, and T. Gustafsson, J. Cryst. Growth **251**, 645 (2003).
[4] A. Giussani, O. Seifarth, P. Rodenbach, H.-J. Müssig, P. Zaumseil, T. Weisemoeller, C. Deiter, J. Wollschläger, P. Storch, and T. Schroeder, J. Appl. Phys. **103**, 084110 (2008).
[5] G. Saint-Girons, P. Regreny, L. Largeau, G. Patriarche, and G. Hollinger, Appl. Phys. Lett. **91**, 241912 (2007).
[6] C. Merckling, M. El-Kazzi, G. Delhaye, M. Gendry, G. Saint-Girons, G. Hollinger, L. Largeau, and G. Patriarche, Appl. Phys. Lett. **89**, 232907 (2006).
[7] T. Schroeder, T. L. Lee, L. Libralesso, I. Joumard, J. Zegenhagen, P. Zaumseil, C. Wenger, G. Lupina, G. Lippert, J. Dabrowski, and H.-J. Müssig, J. Appl. Phys. **97**, 074906 (2005).
[8] T. Schroeder, P. Zaumseil, G. Weidner, C. Wenger, J. Dabrowski, H.-J. Müssig, and P. Storck, J. Appl. Phys. **99**, 014101 (2006).
[9] B. G. Hyde, D. J. M. Bevan, and L. Eyring, Philos. Trans. R. Soc. London, Ser. A **259**, 583 (1966).
[10] D. O. Klenov, L. F. Edge, D. G. Schlom, and S. Stemmer, Appl. Phys. Lett. **86**, 051901 (2005).
[11] A. Schaefer *et al.*, Surf. Sci. **601**, 1473 (2007).
[12] J. Dabrowski and V. Zavodinsky, in *NIC Symposium 2004*, NIC Series, edited by D. Wolf, G. Münster, and M. Kremer (Forschungszentrum Jülich, Jülich, 2003), Vol. 20, p. 171.
[13] S. Hashimoto, J. L. Peng, W. M. Gibson, L. J. Schowalter, and R. W. Fathauer, Appl. Phys. Lett. **47**, 1071 (1985).
[14] B. G. Hyde, E. E. Garver, U. E. Kuntz, and L. Eyring, J. Phys. Chem. **69**, 1667 (1964).
[15] L. Eyring and N. C. Baenziger, J. Appl. Phys. **33**, 428 (1962).
[16] S. Lütkehoff, M. Neumann, and A. Slebarski, Phys. Rev. B **52**, 13808 (1995).

Author complimentary copy. Redistribution subject to AIP license or copyright, see http://apl.aip.org/apl/copyright.jsp